

Supporting Information for

Studies of Pyrroloquinoline Quinone Species in Solution and in Lanthanide-dependent Methanol Dehydrogenases

Nader Al Danaf^{[a,b]†}, Jerome Kretzschmar^{[c]†}, Berenice Jahn^[a], Helena Singer^[a], Arjan Pol^[d], Huub J.M.
Op den Camp^[d], Robin Steudtner^[c], Don C. Lamb^[a,b], Björn Drobot^{*[c]} and Lena J. Daumann^{*[a]}

[a] Department of Chemistry

Ludwig-Maximilians-University Munich

Butenandtstraße 5 – 13, 81377 München (Germany)

[b] Center for NanoScience

Ludwig-Maximilians-University Munich

Geschwister-Scholl Platz 1, 80539 München (Germany)

[c] Institute of Resource Ecology

Helmholtz-Zentrum Dresden-Rossendorf e.V.

Bautzner Landstraße 400, 01328 Dresden (Germany)

[d] Department of Microbiology

Radboud University

Heyendaalseweg 135, 6525 AJ, Nijmegen (The Netherlands)

† Shared first author.

* Corresponding authors: b.drobot@hzdr.de, lena.daumann@lmu.de

Experimental

Enzyme and PQQ preparations: Eu-MDH was purified according to a previously published protocol.¹ La-MDH was purified analogously, however phosphate buffer was used instead of Pipes for enzyme purification and, during cultivation, 5 μM LaCl_3 was used instead of EuCl_3 . PQQ was used as disodium salt that had previously been isolated from vitamin capsules.²

MDH sample preparation for TRLFS: Eu-MDH samples were re-buffered twice in 100 mM NaCl containing 1 mM MeOH and a pH value of 6.5 using a spinfilter (Amicon Ultra, 30 kDa MWCO) run at 4,500 rpm and 4 °C. The protein concentration was determined with a NanoDrop uv/vis spectrophotometer. For the measurement, the concentration was adjusted to 10 μM MDH.

MDH sample preparation for the fluorimeter measurement: MDH was washed twice in 20 mM PIPES pH 7.2 using a spinfilter (Amicon Ultra, 30 kDa MWCO) at 4,500 rpm and 4 °C. The protein concentration was determined with the fiber-optic ultra-micro measuring cell (Traycell). For the measurement, the final concentration was adjusted to 12 μM MDH.

Protonation Constants: The calculation of the protonation constants based on the variation in the absorption spectra were done using the HypSpec program.^{3,4}

Nuclear Magnetic Resonance (NMR) Spectroscopy: PQQ disodium salt was dissolved in Milli-Q water (18.2 M Ω cm), containing 0.1 M NaCl, to yield a 10 mM stock solution (pH = 4.3). Aliquots of the latter were further diluted to 1 mM and pH-adjusted with NaOH and HCl to yield 17 samples with pH values in the range of $0 \leq \text{pH} \leq 4$ with increments of 0.25 pH units. The samples contained 10% D₂O by volume. Due to the lowered solubility upon decreasing pH, PQQ precipitated. Thus, after adjustment to the desired pH value (± 0.05 units), the samples were centrifuged. The clear supernatants – considered as saturated solutions at the given pH – were then used for the NMR measurements.

Samples dedicated for studies at near-neutral and alkaline conditions and micromolar concentrations were prepared by dissolving the appropriate amounts of PQQ disodium salt in 0.1 M NaCl D₂O solution and the pD adjusted using NaOD and DCl.

NMR spectra were recorded on an Agilent DD2-600 system operating at 14.1 T with a corresponding ¹H resonance frequency of 599.82 MHz using a 5 mm oneNMR™ probe.

NMR spectra were measured with 3 s acquisition time after application of a narrow-band 2 s pre-saturation pulse on the water resonance for water signal suppression and a $\pi/6$ observation pulse, accumulating 128 – 2k transitions. For chemical shift determination only (as for pK_a determination), the relaxation delay (d1) was set to 3 s. In the case of quantitative spectra ($d1 \geq 5 \times T_1$), d1 = 20 s was applied for samples with solution pH up to 4.3 while, for samples with pD values of 6.8 and above, d1 was set to 60 s. Since the longitudinal relaxation times are quite long, especially for the pyrrol ¹H nuclei (cf. Table S1), and because of the appropriate signal separation (cf. Figure S2), signals 8 and 8' were used for quantification.

Table S1. Selected relaxation times of aqueous PQQ solutions 10 mM at pH 4.3 and 5 mM at pD 6.8 as determined by the inversion recovery (T_1) and by the Carr–Purcell–Meiboom–Gill (CPMG) pulse sequence (T_2).

		H-8	H-8'	H-3'	H-3
pH 4.3	T_2 / s (25 °C)	0.30 ± 0.01	0.71 ± 0.02	1.32 ± 0.05	1.49 ± 0.02
	T_1 / s (25 °C)	2.8 ± 0.1	3.3 ± 0.1	4.8 ± 0.1	4.8 ± 0.1
	T_1 / s (60 °C)	4.4 ± 0.7	4.8 ± 1.2	6.3 ± 1.2	4.8 ± 0.4
pD 6.8	T_1 / s (25 °C)	10.2 ± 0.5	8.9 ± 0.8	13.4 ± 1.5	14.4 ± 1.2

Fluorescence spectroscopy: Excitation–emission scans were performed on a FluoTime 300 fluorescence spectrometer equipped with a 300 W Xenon arc lamp (PicoQuant). Fluorescence was recorded using a slit width of 2 nm and an integration time of 0.5 s. Emission spectra (425 to 650 nm, 2 nm resolution) were recorded for each excitation wavelength (230 to 420 nm, 3 nm resolution) and combined for each sample to a 2D data matrix. Matrices were stacked to a 3D data cube and analyzed using a parallel factor analysis (PARAFAC) implemented as a N-way toolbox for Matlab⁵ using non-negative constrains for the excitation and emission spectra and the speciation constrain for the distribution described elsewhere.⁶

The time-resolved laser-induced fluorescence spectroscopy (TRLFS) measurements were performed at 4 °C (Eu-MDH) with a pulsed Nd:YAG OPO laser system (Powerlite Precision II 9020 laser with a Green Panther EX OPO, Continuum Electro-Optics, San Jose, USA) equipped with a multi-channel optical analysis system consisting of a Kymera 328i spectrograph and an Andor iStar ICCD camera (both Quantum Design GmbH, Darmstadt, Germany). For the conducted measurements, experiments were performed at an excitation wavelength of 394 nm. The luminescence spectra were recorded in the wavelength range from 500 to 760 nm (grating: 300 lines/mm with a resolution of 0.25 nm). To record the time-dependent luminescence spectra, the delay time between laser pulse and camera control was sampled in dynamic time intervals (usually between 1 and 301 μ s). The recorded 2D sample data were stacked to a 3D data cube. This data cube was analyzed using PARAFAC implemented as a N-way toolbox for Matlab⁵ including an exponential decay constraint⁶. In Eu(III) systems – in the absence of other quenchers – the number of water molecules in the first coordination sphere can be calculated from the luminescence lifetime using the Horrocks equation⁷⁻¹⁰

$$n_{\text{H}_2\text{O}} \pm 0.5 = 1.07 \times k_{\text{exp}} - 0.62 \text{ (Eqn. S1)}$$

Here, n is the number of remaining water molecules and k_{exp} is the decay rate in ms^{-1} ($1/\tau$).

Additional measurements were performed on an FLS 1000 Fluorimeter (Edinburgh Instruments). A pulsed laser diode at 375 nm wavelength (LDH-D-C-375, PicoQuant) was used for excitation of the Eu-

MDH. The dual mode laser head was operated in continuous wave mode for obtaining the steady state emission and the pulsed mode was used for the lifetime measurements. The laser pulses were synchronized in a burst mode of 500 μ s per cycle, in which the laser was pulsed for 5 μ s of this timeframe. The Eu³⁺ luminescence from the Eu-MDH (emission band width of 40 nm centered at 620 nm) was monitored on one channel of the T-geometry of the fluorimeter while the fluorescence of the PQQ (emission band width of 5 nm centered at 495 nm) was monitored on the other channel (H10720-01 High speed PMTs, Hamamatsu, were used for both channels). The fluorescence lifetime measurements were performed on the same FLS 1000 fluorimeter using time-correlated single-photon counting. The raw lifetime data and subsequent lifetime fits were performed with our home written software PIE analysis with Matlab (PAM).¹¹ PAM is a stand-alone program (MATLAB; The MathWorks GmbH) for integrated and robust analysis of fluorescence ensemble, single-molecule, and imaging data. The average fluorescence lifetime (τ_{avg}) values were obtained by using the equation below:

$$\tau_{avg} = (\sum_{i=1}^n \alpha_i \tau_i^2) / (\sum_{i=1}^n \alpha_i \tau_i) \text{ (Eqn. S2)}$$

where τ_i is the individual lifetime with corresponding amplitude α_i .

UV-Vis measurements: Eu-MDH was stored at -80 °C in PIPES buffer (10 mM, pH 7.2) supplemented with 1 mM MeOH and was re-buffered either in NaCl (100 mM, pH 6.5) or in NaCl with 1 mM MeOH for the experiments. Washing of the protein was required due to re-buffering but also to remove degraded protein, pre-used storage buffer, residual methanol, formaldehyde and formic acid from the enzyme. Eu-MDH was transferred to a pre-equilibrated spin filter (Amicon Ultra, 30 kDa MWCO, rinsed twice with MilliQ water and then with the required NaCl solution) with tenfold surplus of the requested buffer and centrifuged (4 °C, 4500 rpm, 15 min). This procedure was repeated once. Measurements were performed on an Agilent Cary 60 UV/Vis spectrophotometer connected to a Peltier element. Spectra were recorded in a micro quartz glass cuvette (Hellma) with a path length of 10 mm after 2 minutes of equilibrium time and manual mixing by pipetting at the set temperature. For all spectra, blank buffer sample was subtracted prior to all measurements as well as a baseline correction at 675 nm was performed. To ensure a comparability of the different treated samples, all spectra were normalized to the total protein absorption peak at 280 nm.

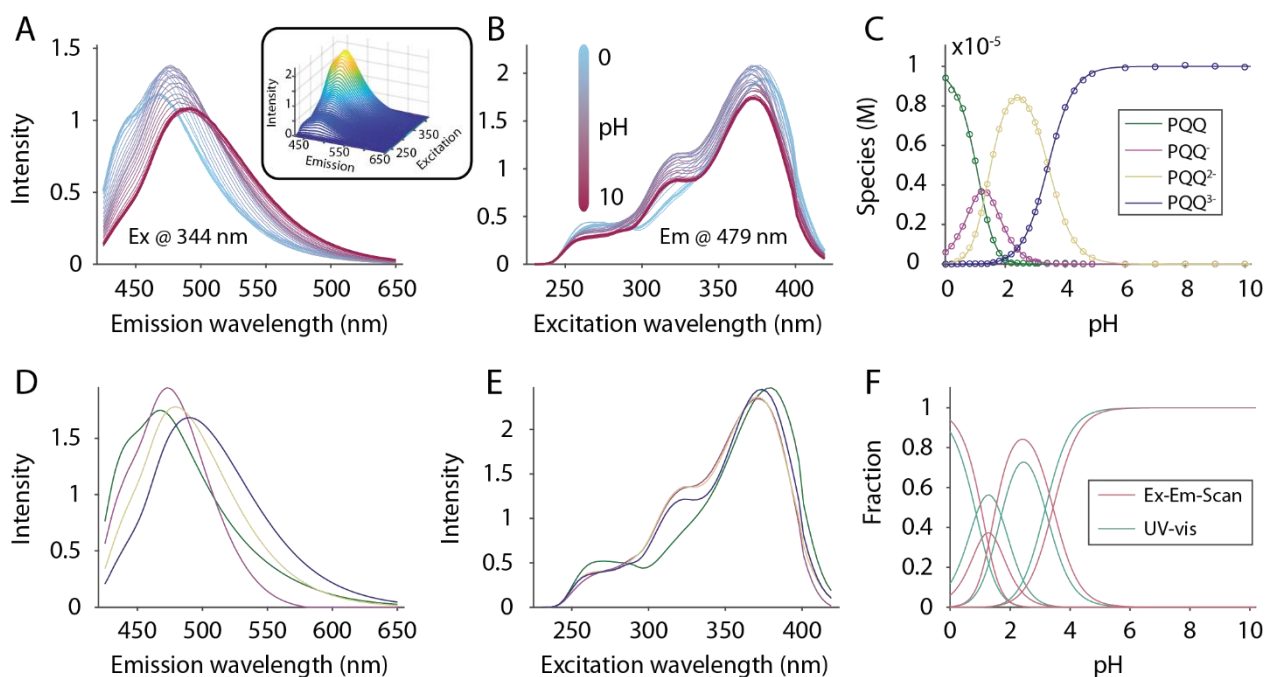


Figure S1 Fluorescence excitation–emission scans of a pH series of 10 μM PQQ in 0.1 M NaCl solution. A complete excitation–emission spectrum of PQQ was recorded for each pH value (inset). Changes in emission (A) and excitation (B) spectra at specific wavelengths demonstrate the sensitivity of the fluorescence to the protonation state. Deconvolution using PARAFAC revealed the population (C), emission spectra (D) and excitation spectra (E) of four different protonation states. The corresponding pK_a values are $pK_{a1} = 1.2$, $pK_{a2} = 1.35$, and $pK_{a3} = 3.4$. This is in good agreement with the extracted values from UV-vis, which is proven by similar calculated speciation based on the pK_a values (F)

Water Adduct Equilibrium: Formation of the water adduct can be expressed by the following reaction equation:



Since water acts as both solvent and reactant, and is thus in large excess, its activity can be assumed to remain constant during the reaction and is set equal to unity. Since the overall concentration of PQQ is sufficiently low, the law of mass action can be written as:

$$K_h = \frac{[\text{PQQ}\cdot\text{H}_2\text{O}]}{[\text{PQQ}]} \text{ (Eqn. S4)}$$

where K_h denotes the equilibrium constant for the hydration reaction and the square brackets denote (relative) concentrations determined from the spectral deconvolution.

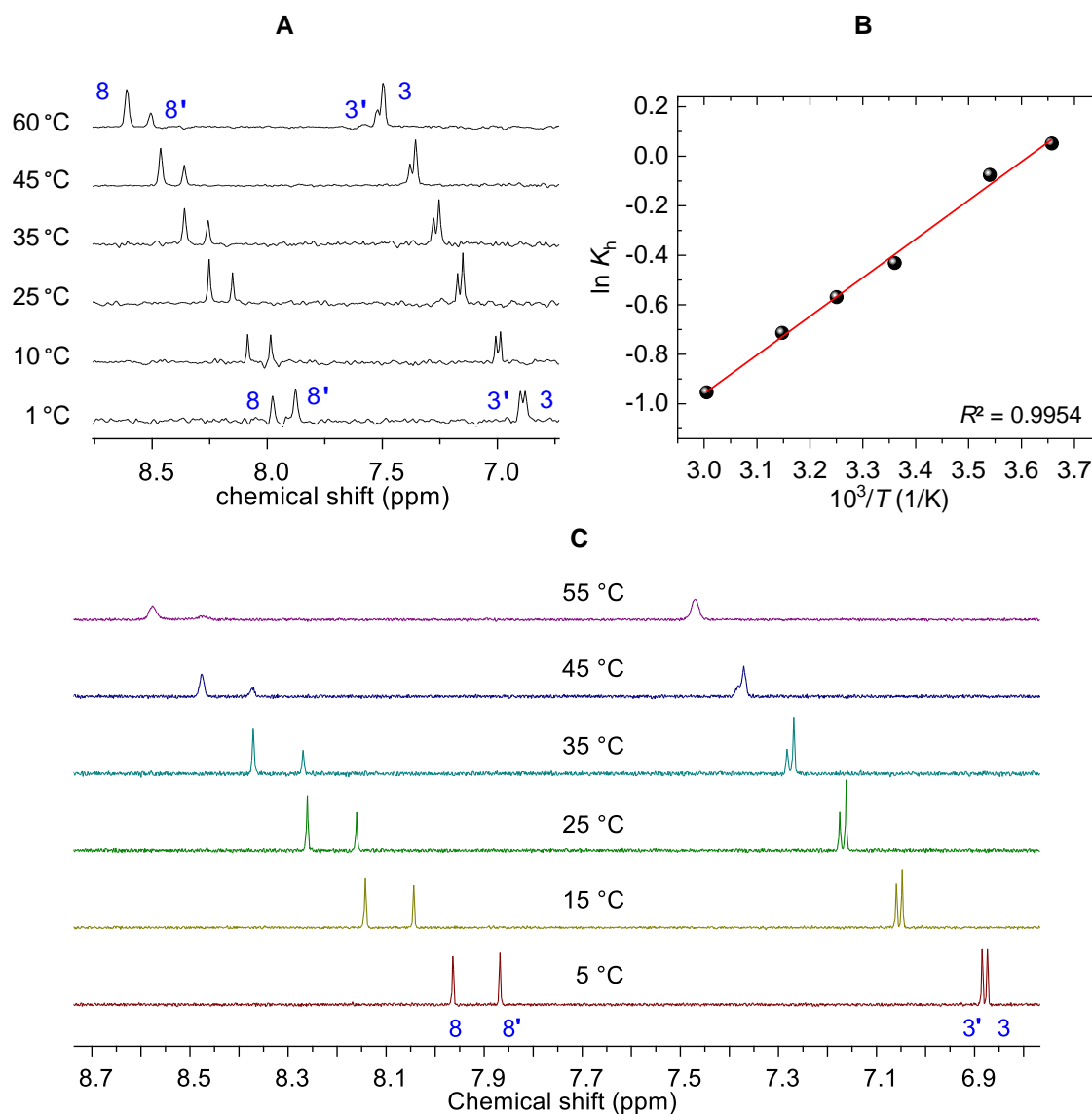


Figure S2. Quantitative ¹H NMR spectra of 1 mM PQQ in 100 mM NaCl pH 4.0 90/10 (v/v) H₂O/D₂O solution acquired at different temperatures (A) and the corresponding van 't Hoff plot (B), where ln K_h was determined as shown in Eqn. S5. (C) Temperature-dependent ¹H NMR spectra of 0.5 mM PQQ in 100 mM NaCl pD 6.8 D₂O solution together with signal assignment, with prime notation for PQQ•H₂O. Note that, for the given pD conditions, both forms occur solely in their tri-anionic species.

By means of the relationship

$$\ln K_h = \frac{-\Delta_h H}{R} \frac{1}{T} + \frac{\Delta_h S}{R} \text{ (Eqn. S5),}$$

the enthalpy and entropy of hydration, $\Delta_h H$ and $\Delta_h S$ respectively, can be calculated. R denotes the molar gas constant ($\sim 8.3145 \text{ J mol}^{-1} \text{ K}^{-1}$) and T represents the absolute temperature.

The absolute concentration appears to have only a minor influence on the K_h as concluded from the K_h determinations for PQQ with total concentrations of 0.5 mM (Figure 4, black data points) and 5 mM (Figure 4, red data point; the corresponding spectrum is shown in red in the inset) at pH 6.8. PQQ's

speciation is directly associated with the decreasing electrophilicity of C(5). Starting at high $[H^+]$, equivalent to low pH, PQQ dominates as the neutral $H_3PQQ_{(aq)}$ species. Upon increasing pH, successive deprotonation yields H_2PQQ^- , $HPQQ^{2-}$, and finally PQQ^{3-} (for the considered pH range up to pH 10; Figure 5). This stepwise deprotonation is accompanied by an increase in negative charges, which is well mirrored by the increasing shielding of all 1H nuclei, corresponding to decreasing chemical shift values (Figure 2 and inset in Figure 6). Increasing the number of negative charges in the PQQ molecule reduces the electrophilicity of C(5), *i.e.* increases its local electron density, thereby reducing the affinity to be attacked by a nucleophile. Consequently, increasing pH shifts the equilibrium towards PQQ.

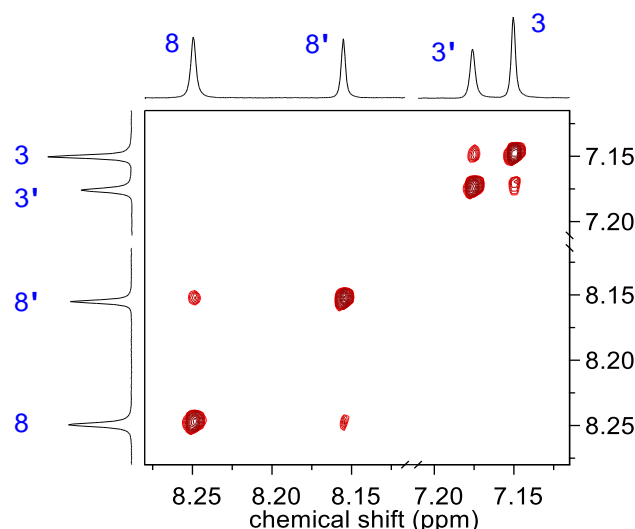


Figure S3 Exemplary quantitative H,H-EXSY spectrum of a 10 mM PQQ aqueous solution containing 10% D_2O at pH 4.3, acquired with 1500 ms mixing time at 25 °C. Signal labeling is according to the atomic numbering in Figure 1, with prime notation for $PQQ \cdot H_2O$.

The correlation (off-diagonal) signals in Figure S3 unambiguously demonstrate the chemical exchange between the two PQQ forms of interest. According to Perrin and Dwyer,¹² evaluation of the volume integrals of the EXSY spectrum allows for the extraction of the rate constant.

$$k_{ex} = \frac{1}{t_{mix}} \ln \frac{q+1}{q-1} \quad (\text{Eqn. S6})$$

$$\text{where } q = 4x_A x_B (I_{AA} + I_{BB}) / (I_{AB} + I_{BA}) - (x_A x_B)^2 \quad (\text{Eqn. S7})$$

and where t_{mix} is the mixing time, x_i is the mole fraction of form i , and I_{ii} and I_{ij} are the volume integrals of the diagonal and the off-diagonal signals, respectively. Taking the EXSY volume integrals obtained for $t_{mix} = 1500$ ms (Figure S3) and $t_{mix} = 500$ ms (not shown), and the mole fractions obtained from quantitative $1D^{-1}H$ measurements, the rate constant for the chemical exchange is $k_{ex}(25 \text{ } ^\circ\text{C}) = (2.0 \pm 0.1) \times 10^{-1} \text{ s}^{-1}$.

From

$$K_h = r_{hyd}/r_{deh} \quad (\text{Eqn. S8}),$$

$$X_{\text{PQQ}} r_{\text{hyd}} = X_{\text{PQQ} \cdot \text{H}_2\text{O}} r_{\text{deh}} \quad (\text{Eqn. S9}), \text{ and}$$

$$k_{\text{ex}} = r_{\text{hyd}} + r_{\text{deh}} \quad (\text{Eqn. S10})$$

follows that

$$r_{\text{hyd}} = X_{\text{PQQ} \cdot \text{H}_2\text{O}} k_{\text{ex}} \quad (\text{Eqn. S11}) \text{ and}$$

$$r_{\text{deh}} = X_{\text{PQQ}} k_{\text{ex}} \quad (\text{Eqn. S12})$$

where r_{hyd} and r_{deh} are the apparent rates of the hydration (forward) and dehydration (backward) reaction, respectively.

The 2D-EXSY is a quite time-consuming experiment – in this case about three days – owing to the quantitative acquisition conditions, the rather long spin-lattice relaxation times (T_1) (cf. Table S1), the slow exchange rate and the thus required long mixing times. Therefore, another approach was used for exchange rate determination, viz. the one-dimensional 1D-EXSY, applying a double-pulsed field gradient spin echo sequence for narrow band excitation. After selective excitation of 8-H (ζ), the peak evolving from dynamic exchange, 8', corresponding to the correlation signal in the 2D experiment, will rise in intensity for increasing mixing times, see Figure S4.

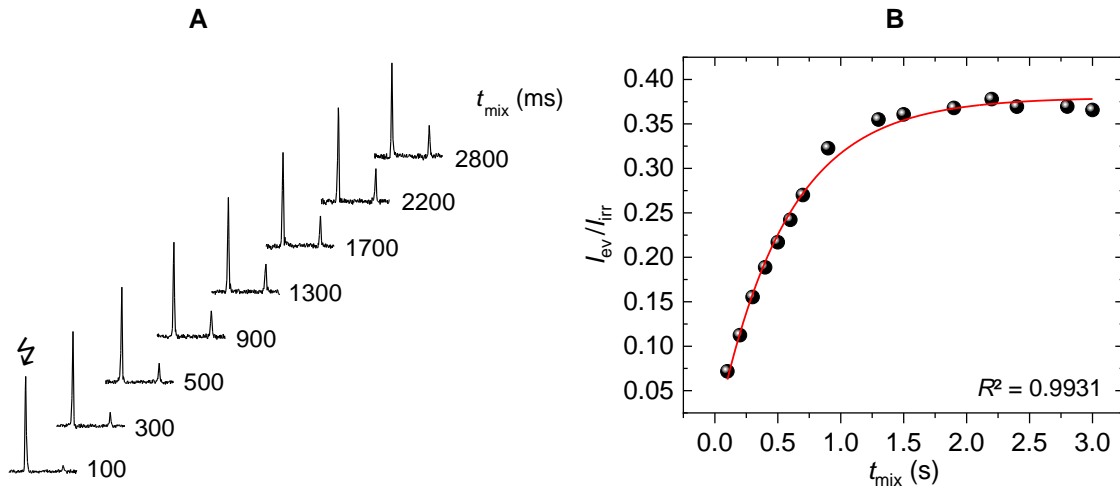


Figure S4. (A) Exemplary selective 1D-EXSY spectra of a 10 mM pH 4.3 PQQ sample acquired at 60 °C for different mixing times, t_{mix} , normalized to the signal being irradiated (ζ). (B) Ratio of the intensities of the evolved and irradiated signal as a function of the applied mixing time.

The obtained spectra were integrated by spectral deconvolution and the ratio of the integrals of the evolving and irradiated signals ($I_{\text{ev}}/I_{\text{irr}}$) plotted against the respectively applied mixing times. For determination of the exchange rate constant, the data were fitted according to:

$$\frac{I_{\text{ev}}}{I_{\text{irr}}} = \left(\frac{I_{\text{ev}}}{I_{\text{irr}}} \right)_0 (1 - e^{-k_{\text{ex}} t_{\text{mix}}}) \quad (\text{Eqn. S13})$$

where $(I_{\text{ev}}/I_{\text{irr}})_0$ is the respective ratio without irradiation, corresponding to K_{h} for the given temperature. The thus calculated exchange rate constant, $k_{\text{ex}}(60 \text{ } ^\circ\text{C})$, amounts to $(18.0 \pm 0.4) \times 10^{-1} \text{ s}^{-1}$. This value

is considered reliable since the method for determination is very robust, and is in excellent agreement with the related value determined from 2D-EXSY at 60 °C (Table 1). The corresponding values for 35 °C and 45 °C were obtained analogously and are also reported in Table 1.

As per *transition state theory*, rate constants determined at different temperatures allow for the calculation of Gibbs energy of activation ΔG^\ddagger , as well as the so-called activation parameters enthalpy and entropy of activation, ΔH^\ddagger and ΔS^\ddagger , respectively, which are related corresponding to

$$k_{\text{ex}}(T) = \frac{k_{\text{B}}T}{h} \exp\left\{\frac{-\Delta H^\ddagger}{RT}\right\} \exp\left\{\frac{\Delta S^\ddagger}{R}\right\} \text{ (Eqn. S14)}$$

where h is Planck's constant ($\sim 6.626 \times 10^{-34}$ J s), and k_{B} is the Boltzmann constant ($\sim 1.381 \times 10^{-23}$ J K⁻¹).

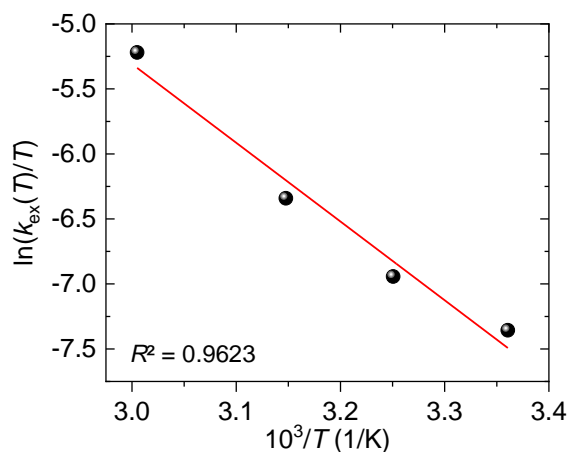


Figure S5. Eyring plot obtained from temperature-dependent exchange rates as determined by exchange spectroscopies for the 10 mM PQQ (100 mM NaCl) pH 4.3 solution.

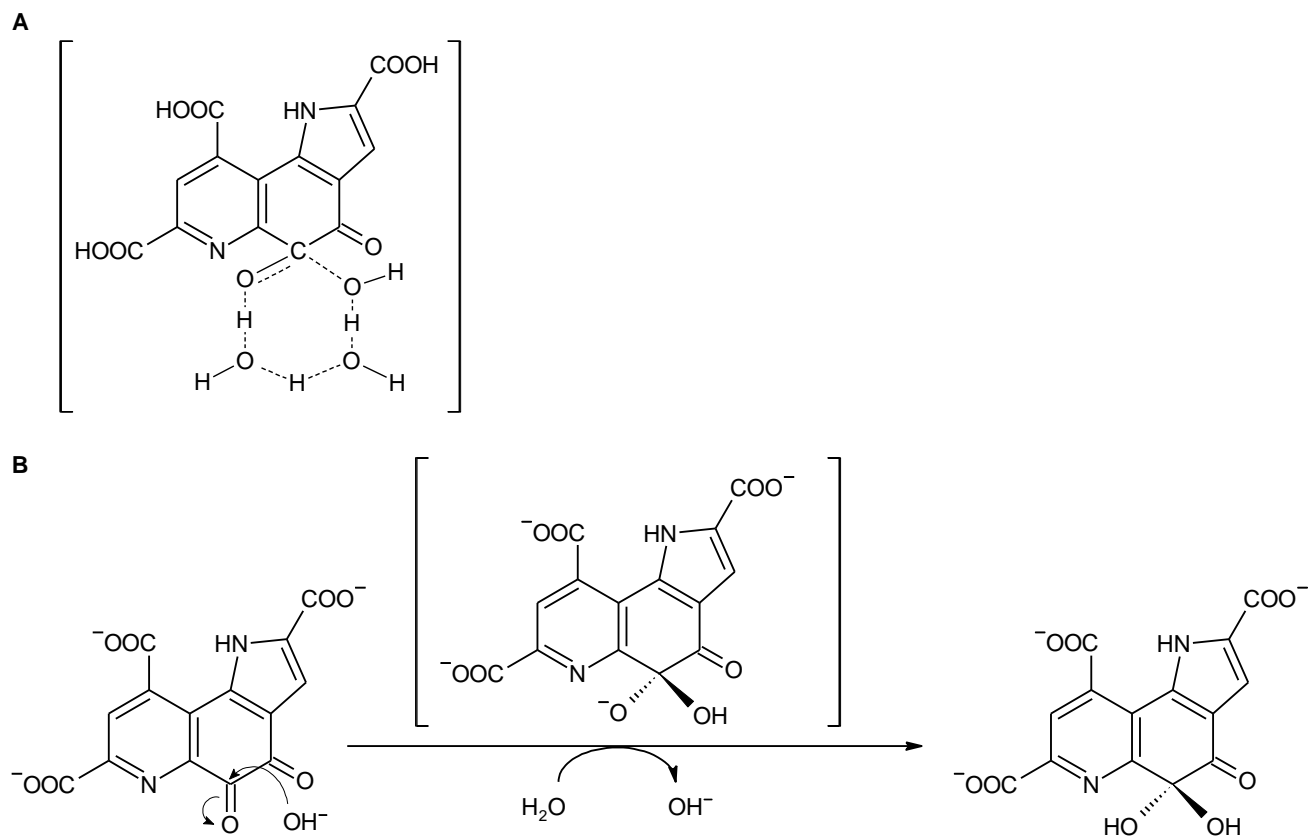


Figure S6. Suggested structure of the highly ordered cyclic hydrogen-bonded transition state for water adduct formation to carbon C(5) for sufficiently low pH where water is the nucleophile (A), and sketched reaction for water adduct formation to carbon C(5) via tetrahedral transition state where the hydroxide ion acts as the nucleophile (B).

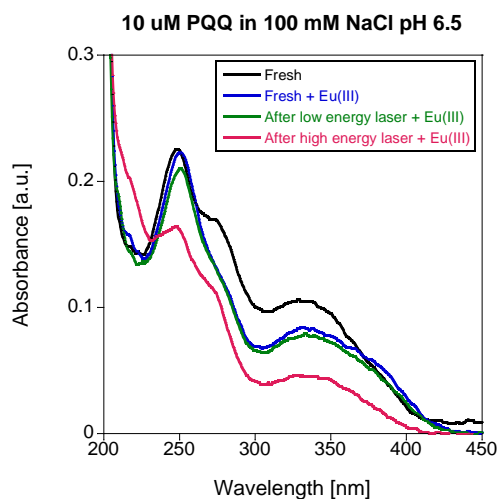


Figure S7. UV-Vis spectra of PQQ with added EuCl_3 before and after irradiation for 1 hour with different laser powers (between 0.1 and 1.4 mJ per pulse) to determine the appropriate laser power for the TRLFS experiments. Spectra were collected at room temperature in 100 mM NaCl solution at pH 6.5.

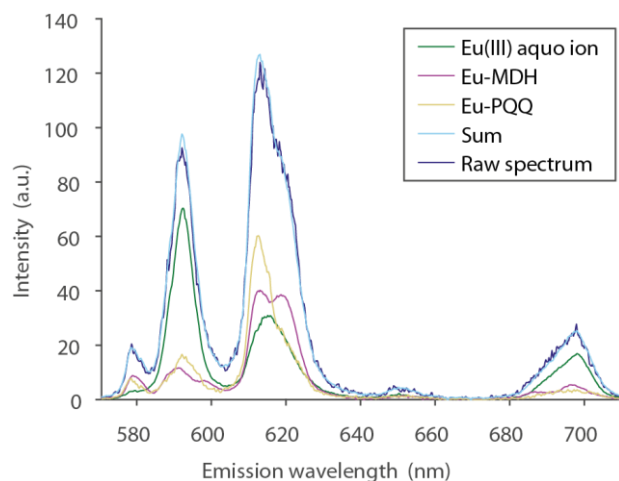


Figure S8. Example of the deconvolution of the emission spectrum of 40 μM EuCl_3 in 100 mM NaCl at pH 6.5. The raw spectrum (dark blue) is well reproduced by the sum (light blue) of the individual species (green, magenta, yellow).

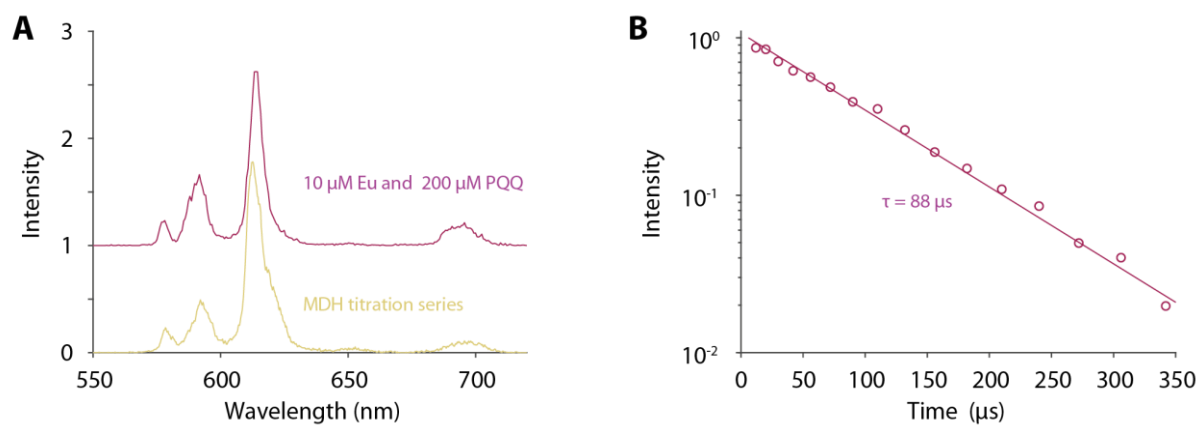


Figure S9. Comparison of the emission spectrum of species 3 from Figure 8 in the main text (yellow) with an emission spectrum obtained from TRLFS of Eu(III) complexed with PQQ (magenta). The assignment of species 3 to a PQQ-bound Eu(III) species is further supported by their luminescence lifetimes. Both show significant quenching compared to the Eu(III) -aquo ion.

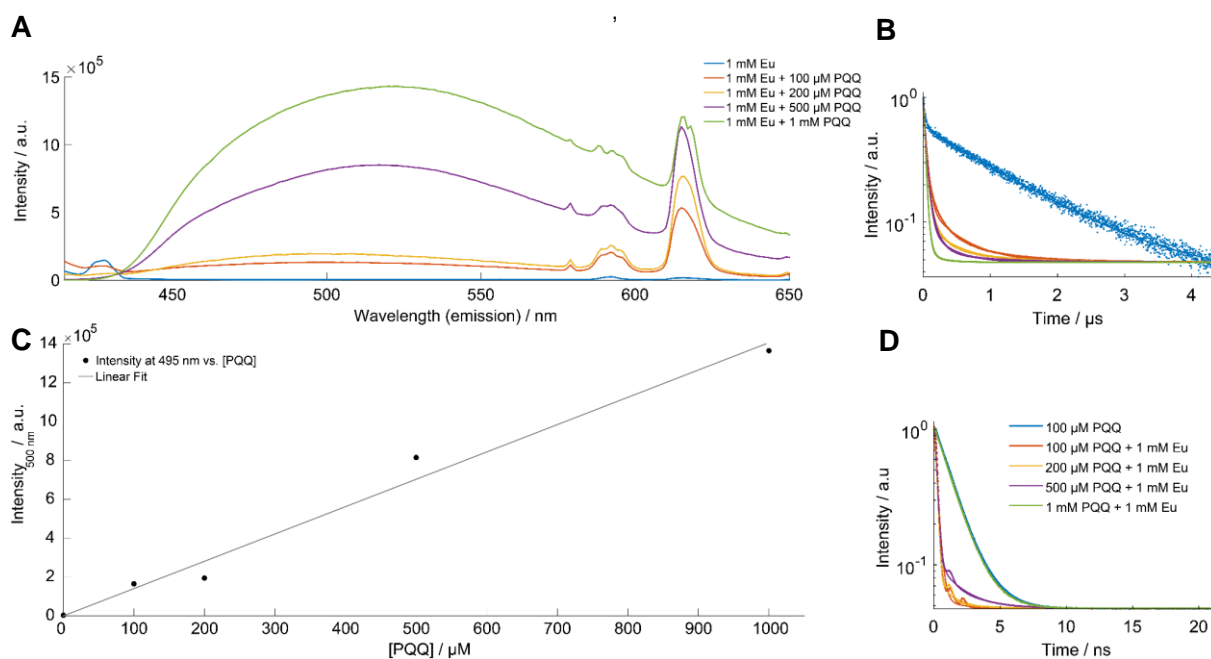


Figure S10. Titration of PQQ to 1 mM Eu in 20 mM PIPES. A) Steady-state luminescence emission spectra with 375 nm excitation for the PQQ titrated Eu(III) sample. B) The Eu luminescence lifetime decay on the μs timescale monitored at 620 nm. C) PQQ intensity (monitored at 495 nm) vs. [PQQ] and D) the fluorescence lifetime of PQQ monitored at 495 nm during the titration series.

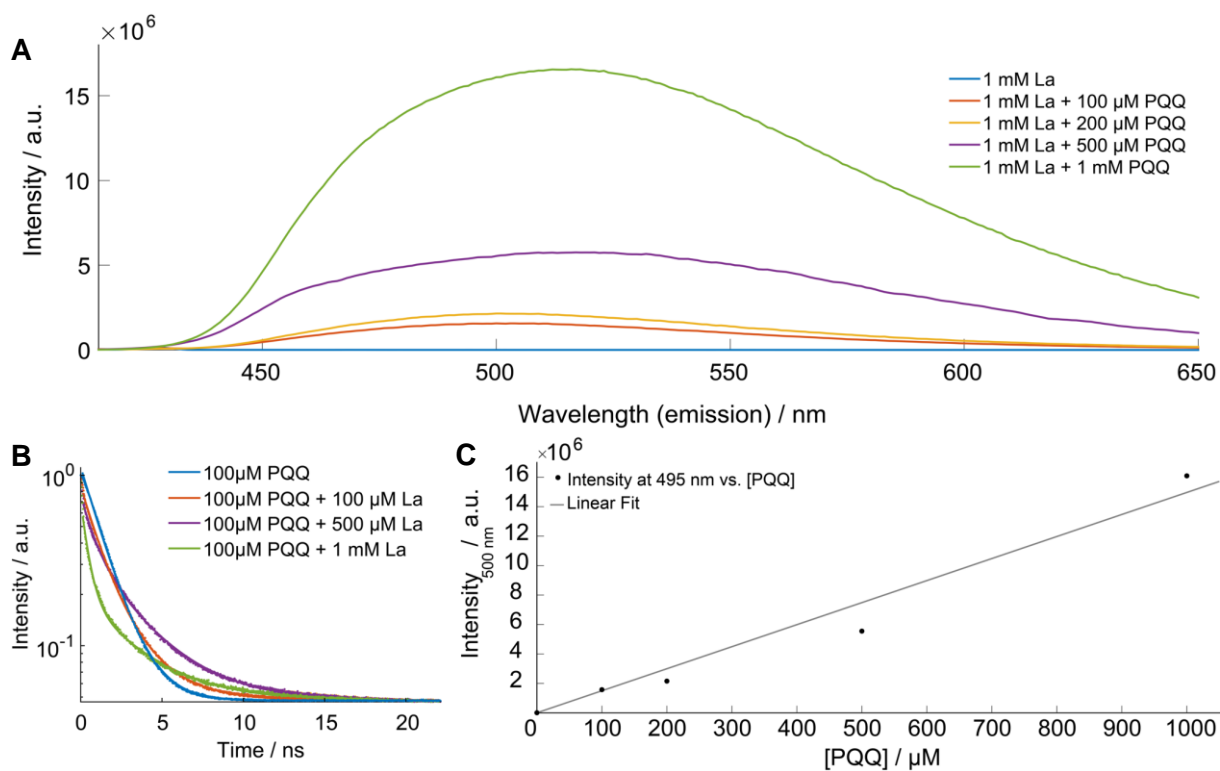


Figure S11. Titration of PQQ to 1 mM La in 20 mM PIPES. A) Steady-state luminescence emission spectra with 375 nm excitation of 1 mM La upon titration with PQQ. B) The fluorescence lifetime of PQQ monitored at 495 nm is plotted during the titration series and C) the PQQ intensity (monitored at 495 nm) is plotted versus [PQQ].

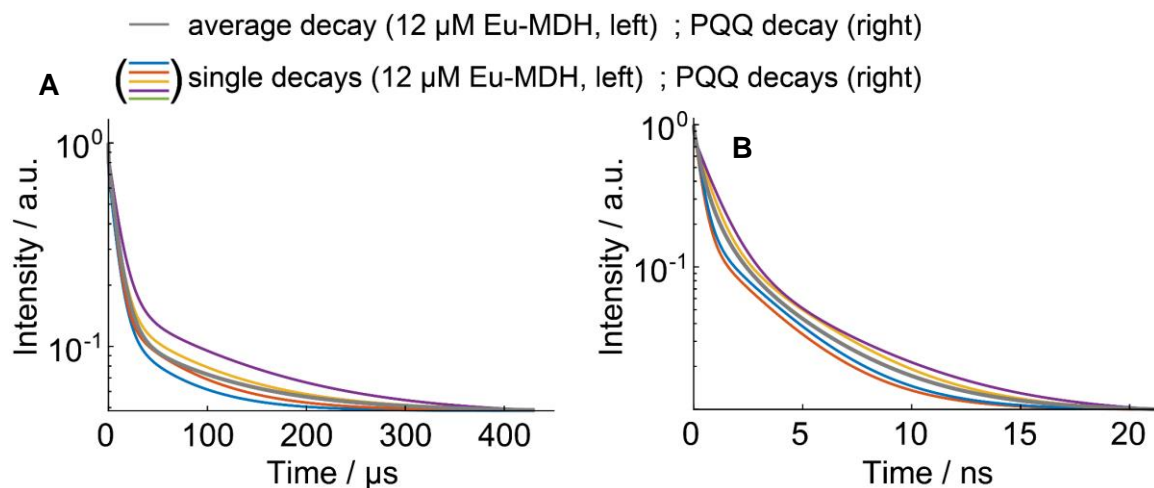


Figure S12 Sample variability. A) The luminescence lifetime of Eu(III) monitored at 620 nm and B) PQQ fluorescence decay after 375 nm excitation is plotted for various sample preparations. The individual decay curves (colored) and the averaged decay (grey) are shown. The variation in the amount of energy transferred indicates differences in the Eu(III) occupancy of the active site of MDH.

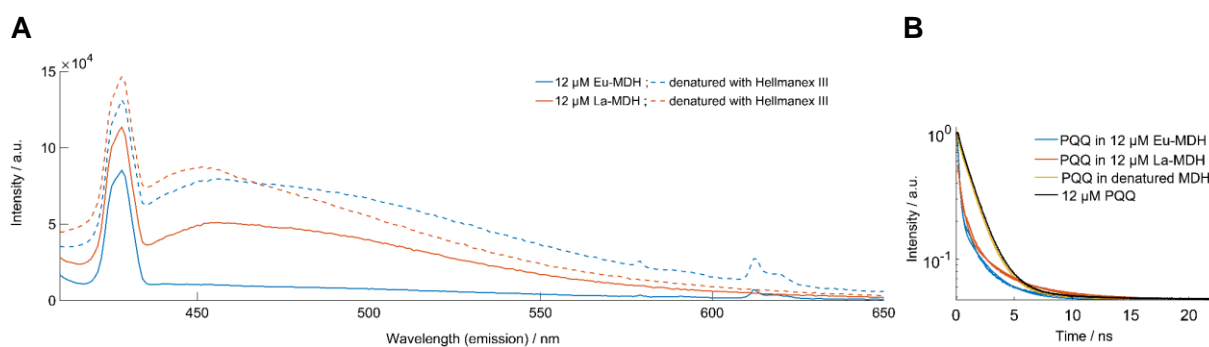


Figure S13. Luminescence emission spectra of the Eu-MDH and La-MDH enzymes in 20 mM PIPES before and after denaturation. A) Steady-state luminescence emission spectra with 375 nm excitation for Eu-MDH and La-MDH are shown. B) The fluorescence lifetime of PQQ in the Eu-MDH and La-MDH monitored at 495 nm are plotted before and after denaturation.

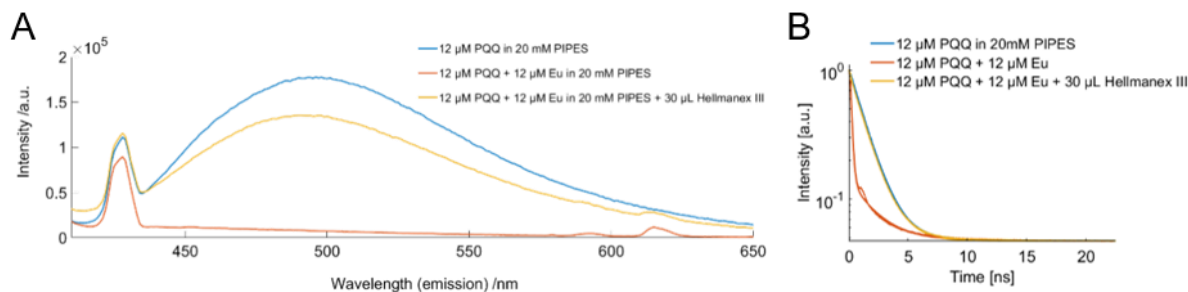


Figure S14. PQQ in 20 mM PIPES upon the addition of Eu and afterwards Hellmanex, as a control tested under similar concentrations to the Eu-MDH. A) Steady-state luminescence emission spectra with 375 nm excitation of PQQ in 20 mM PIPES before and after addition of Eu and Hellmanex III. B) The corresponding fluorescence lifetime of PQQ monitored at 495 nm is plotted during the measurements.

References

1. B. Jahn, A. Pol, H. Lumpe, T. R. M. Barends, A. Dietl, C. Hogendoorn, H. J. M. Op den Camp and L. J. Daumann, *ChemBiochem*, 2018, **19**, 1147-1153.
2. H. Lumpe and L. J. Daumann, *Inorg. Chem.*, 2019, **58**, 8432-8441.
3. P. Gans, A. Sabatini and A. Vacca, *Talanta*, 1996, **43**, 1739-1753.
4. P. Gans, A. Sabatini and A. Vacca, *Ann. chim*, 1999, **89**, 45-49.
5. C. Andersson and R. Bro, *Chemom. Intell. Lab. Syst.*, 2000, **52**, 1-4.
6. B. Drobot, A. Bauer, R. Steudtner, S. Tsushima, F. Bok, M. Patzschke, J. Raff and V. Brendler, *Anal. Chem.*, 2016, **88**, 3548-3555.
7. W. D. Horrocks and D. R. Sudnick, *J. Am. Chem. Soc.*, 1979, **101**, 334-340.
8. T. Kimura and Y. Kato, *J. Alloys Compd.*, 1998, **275-277**, 806-810.
9. P. P. Barthelemy and G. R. Choppin, *Inorg. Chem.*, 1989, **28**, 3354-3357.
10. T. Kimura and G. R. Choppin, *J. Alloys Compd.*, 1994, **213-214**, 313-317.
11. W. Schrimpf, A. Barth, J. Hendrix and D. C. Lamb, *Biophys. J.*, 2018, **114**, 1518-1528.
12. C. L. Perrin and T. J. Dwyer, *Chem. Rev.*, 1990, **90**, 935-967.